



## City Research Online

### City, University of London Institutional Repository

---

**Citation:** Stefanidou, S.P. & Kappos, A. J. (2017). Methodology for the development of bridge-specific fragility curves. *Earthquake Engineering and Structural Dynamics*, 46(1), pp. 73-93. doi: 10.1002/eqe.2774

This is the accepted version of the paper.

This version of the publication may differ from the final published version.

---

**Permanent repository link:** <https://openaccess.city.ac.uk/id/eprint/16023/>

**Link to published version:** <https://doi.org/10.1002/eqe.2774>

**Copyright:** City Research Online aims to make research outputs of City, University of London available to a wider audience. Copyright and Moral Rights remain with the author(s) and/or copyright holders. URLs from City Research Online may be freely distributed and linked to.

**Reuse:** Copies of full items can be used for personal research or study, educational, or not-for-profit purposes without prior permission or charge. Provided that the authors, title and full bibliographic details are credited, a hyperlink and/or URL is given for the original metadata page and the content is not changed in any way.

---

---

---

City Research Online:

<http://openaccess.city.ac.uk/>

[publications@city.ac.uk](mailto:publications@city.ac.uk)

---

# Methodology for the development of bridge-specific fragility curves

Sotiria P. Stefanidou<sup>1</sup> and Andreas J. Kappos<sup>1,2</sup>

<sup>1</sup> Department of Civil Engineering, Aristotle University of Thessaloniki

<sup>2</sup> Department of Civil Engineering, City University London

## SUMMARY

A new methodology for the development of bridge-specific fragility curves is proposed with a view to improving the reliability of loss assessment in road networks and prioritizing retrofit of the bridge stock. The key features of the proposed methodology are the explicit definition of critical limit state thresholds for individual bridge components, with consideration of the effect of varying geometry, material properties, reinforcement and loading patterns on the component capacity; the methodology also includes the quantification of uncertainty in capacity, demand, and damage state definition. Advanced analysis methods and tools (nonlinear static analysis and incremental dynamic response history analysis) are used for bridge component capacity and demand estimation, while reduced sampling techniques are used for uncertainty treatment. Whereas uncertainty in both capacity and demand is estimated from nonlinear analysis of detailed inelastic models, in practical application to bridge stocks the demand is estimated through a standard response spectrum analysis of a simplified elastic model of the bridge. The simplified methodology can be efficiently applied to a large number of bridges (with different characteristics) within a road network, by means of an ad-hoc developed software involving the use of a generic (elastic) bridge model, that derives bridge-specific fragility curves.

**KEY WORDS:** Bridges; fragility curves; damage states; uncertainty analysis; nonlinear analysis; loss estimation; road network.

## 1. INTRODUCTION

Damage due to recent earthquakes worldwide highlights the role of bridges as arguably the most vulnerable component of a road or railway system. In view of this, during the last two decades, several methodologies have been developed for the assessment of bridge vulnerability, mainly in the context of developing fragility curves [1]. Since fragility is the probability that bridge damage exceeds a specific limit state (damage state) threshold for a given level of earthquake intensity, the key issues, within all the methodologies available in the literature, are the probabilistic seismic demand model assumed, the intensity measure used for fragility analysis, the selection of engineering demand parameters (EDPs) and relevant limit state thresholds for capacity estimation, the analysis method for demand estimation, the correlation of system and critical component damage, and, finally, the treatment of uncertainty.

Multiple bridge components, namely piers, bearings, abutments and foundations, are commonly considered during the assessment of seismic performance and estimation of bridge system fragility [2], although consideration of a single critical component (i.e. bridge piers) has also been an option [3]. Either way, the differentiation among existing methodologies lies primarily on damage definition, since component damage may be directly related to system limit states using global engineering demand parameters and fragility can be estimated directly at

system level thereafter [4], or be defined using local EDPs for each component independently, and component fragility can be related to system fragility assuming a certain correlation between multiple components [5] (i.e. joint probabilistic seismic demand models, series or parallel connection of components [6], [7]).

Several engineering demand parameters (local or global) were proposed for the quantitative definition of damage in critical components, based on experimental results [8, 9] while multiple failure modes of components were also taken into consideration [10]. It has to be pointed out that in most cases the available values of local EDPs do not cover the range of all possible pier types, and even when they do [10], they concern solely the serviceability and ‘ultimate’ limit state (member failure), which may result in conservative assessment of bridge damage and functionality.

Numerous analysis methods were proposed for demand evaluation, covering a range of levels of complexity and computational cost. In particular, elastic response spectrum analysis [11] and inelastic pushover analysis of a detailed inelastic model [4], or a simplified single-degree-of-freedom model [2] (e.g. capacity spectrum method [12]) are common options. Notwithstanding its computational cost, non-linear response history analysis is broadly considered to be the most rigorous and reliable method for demand estimation [13]. Therefore, this method was applied in various methodologies available in the literature [14, 6, 7], using appropriately selected accelerograms consistent with the probabilistic seismic demand model considered, i.e. the cloud approach or incremental dynamic analysis (IDA).

The evaluation of the total uncertainty in a fragility curve requires the quantification of uncertainty in capacity, demand and damage state definition [15, 16], considering all uncertainty sources (aleatory and epistemic [17]). Uncertainty in capacity estimation is in principle defined on the basis of experimental results [8]; alternatively, numerical analysis of a statistically reliable sample can be used [14], adopting statistical models for the materials available in the literature. Uncertainty in demand is typically evaluated through inelastic analysis of bridge models, assuming randomness in the ground motion suite along with bridge modelling and parameter uncertainties [7].

The probability distribution of the response can be analytically derived from functional relationships of the random input variables using metamodels, therefore, in this case, no a priori assumption for the type of demand distribution is necessary [18]. Alternatively (and in most cases), each component demand is represented by a probabilistic seismic demand model (cloud approach or IDA), estimating the parameters of the lognormal distribution of demand through regression analysis [6, 7]. It is also noted that the logarithmic mean and dispersion value could be estimated simultaneously using the maximum likelihood method [19].

The selection of the optimal intensity measure (IM) for fragility analysis is a rather controversial and case-dependent issue. Several researchers argue that spectral parameters at the fundamental period of the bridge are the most appropriate, since they tend to reduce uncertainty in the demand model, whereas others [4, 20] believe that (the historically used) peak ground acceleration (PGA) is a proper choice.

A key drawback of the existing methodologies is that they are either based on advanced analysis tools, increasing dramatically the computational cost when applied to a large bridge stock, or on approximate methods that do not account for the seismic performance of all critical structural components, hence risking to miss potential failure modes in some cases. Moreover, the main goal of the available methodologies, irrespective of considering multiple or single critical components, is to provide fragility curves for particular bridge types and structural systems (typical bridges of specific categories, defined on the basis of a selected classification

system [9]), hence reducing the reliability of loss assessment when these are applied to bridge stocks that include bridges with substantial variability in the properties of bridges assigned to a certain class. Furthermore, the majority of existing methodologies do not account for the effect of bridge-specific component properties on capacity, limit state thresholds, demand and, eventually, system fragility. Although the effect of bridge properties on pier capacity is recognised and closed-form relationships were proposed in [21] for the quantification of bridge capacity, uniform limit state thresholds are commonly proposed, ignoring the effect of bridge structural properties on damage thresholds and failure modes. Finally, it should be noted that in most cases uncertainties in demand and capacity are considered in a ‘lumped’ way, rather than being defined for individual key components of the bridge.

In the context of the foregoing review, the key objective of this paper is to put forward a new methodology for the derivation of bridge-specific fragility curves, feasible for application to a bridge stock of realistic size, with a view to estimating seismic losses in the bridges, as well as in the road network [22]; the latter aspect is part of the same study, but is not further addressed herein. In general, bridges in a road network have different geometries, structural systems and component properties, due to differences in the topography and the construction method selected. Therefore, the proposed methodology aims to reconcile two conflicting requirements, namely the need for a detailed and reliable estimation of bridge capacity, demand and the associated uncertainties, as well as the broad and efficient application. To this end, the backbone of the proposed methodology is the development of a database, including critical bridge components and a variety of geometric, material, reinforcement and loading patterns, in order to explicitly define the case-dependent component capacity and limit state thresholds. The inherent correlation of component properties and limit state thresholds is recognised; therefore empirical relationships are proposed to quantify component capacity limits for different performance levels in terms of global engineering demand parameters (relating local to global damage), considering different boundary conditions (pier-to-deck connection) and failure modes. Furthermore, component demand for different levels of earthquake intensity is calculated based on either a detailed inelastic or a simplified elastic model, and multiple stripe (enhanced IDA) or response spectrum analysis, respectively, according to the desired level of accuracy and computational cost (related to whether a single bridge or a bridge stock is addressed). Component fragility is then calculated and is used to estimate system fragility (of the entire bridge), assuming series connection between components. Finally, in the frame of the proposed methodology, the uncertainty in demand, component capacity, and limit state definition are explicitly defined for each component and limit state, while a total uncertainty value is also proposed for different bridge types.

## 2. METHODOLOGY FOR THE DERIVATION OF BRIDGE-SPECIFIC FRAGILITY CURVES

The methodology proposed herein consists of three distinct ‘steps’ (each consisting of a number of actions), considering the definition of capacity thresholds for the quantification of component damage and the associated uncertainties, the calculation of component demand and the uncertainties in demand estimation and, finally, the correlation of component fragilities to evaluate system fragility for various levels of earthquake intensity. It is important to note that the procedure (in particular Step 2) is different when a single bridge or a bridge stock (typically that in the road or railway network analysed) is considered. The basic procedure followed at each step is outlined in the following.

*Step 1: Component limit state thresholds (capacity) and associated uncertainty*

In the general case of a bridge stock the procedure is as follows:

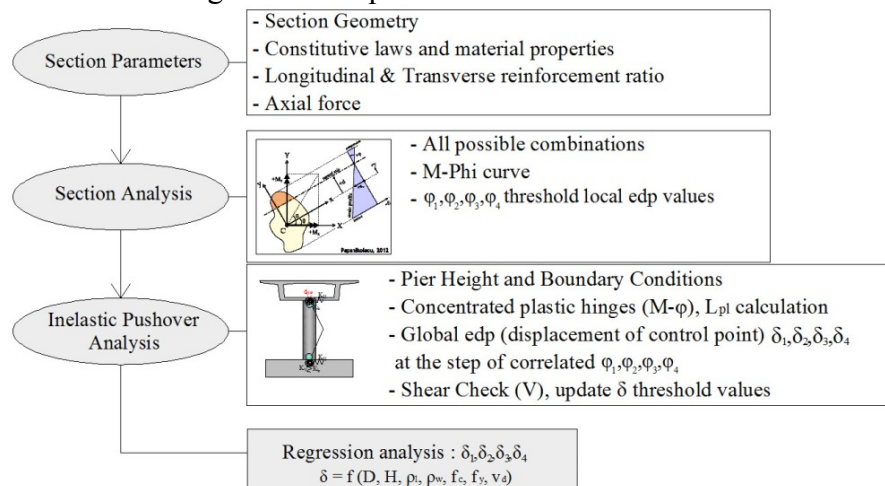


Figure 1. Component (pier) limit state thresholds in displacement terms

- Definition of the basic configurations of critical bridge components (piers, bearings, abutments) for the bridge stock.
- Compilation of a database consisting of different *pier* section types, with varying geometric, material, reinforcement and loading patterns.
- Definition of pier limit state thresholds (for all pier sections in the database) using a local engineering demand parameter, by means of section analysis and correlation of material strain (related to crack width) to section curvature (local damage parameter).
- Consideration of a sufficiently broad range of heights for each pier section type, developing a database that encompasses practically all bridge piers found in the studied bridge stock.
- Definition of pier capacity limit state thresholds in terms of a global engineering demand parameter (displacement), correlated to local damage (pier critical section) by means of inelastic pushover analysis of the equivalent cantilever (pier segment up to contraflexure point); multiple failure modes (flexural and shear) and P-delta effects are considered. Empirical relationships for the calculation of component-specific limit state thresholds (in terms of displacement) are derived for all pier types, accounting for the effect of different component characteristics on component capacity.
- Correlation of threshold values calculated in terms of displacement at the control point (tip of equivalent cantilever), to the displacement at the top of a pier having specific boundary conditions (pier connection to the deck and the foundation). An analytical expression for the correlation of equivalent cantilever displacement to the displacement at the top of the actual pier is proposed (section 2.1).
- Definition of limit state thresholds for *bearings*, in terms of a global engineering demand parameter, based primarily on experimental data.
- Definition of limit state thresholds for *abutments*, in terms of a global engineering demand parameter, based on available proposals in the literature and nonlinear analysis of the critical part of the abutment (the backwall).
- Consideration of material properties, ultimate concrete strain, and plastic hinge length ( $L_{pl}$ ) as random variables and application of a reduced sampling technique, such as Latin Hypercube Sampling [23], for the quantification of uncertainty in capacity ( $\beta_c$ ) for all pier types studied.

- (j) Estimation of uncertainty in limit state definition ( $\beta_{LS}$  for capacity thresholds), critically considering the range of values proposed in the literature and calculating the dispersion (adopting the assumption of lognormal distribution).

The basic aspects of ‘step’ 1 are summarised in Figure 1 for the case of piers; similar, but less involved, procedures apply for abutments and bearings. When a single bridge is analysed, this step consists in the definition of the properties of piers, abutments and bearings, and their pushover analysis, taking uncertainty in properties into account and hence determining the uncertainty in capacity thresholds.

### *Step 2: Component demand and associated uncertainty*

Depending on the purpose of the study, i.e. whether a single bridge is fully analysed (including also the uncertainty quantification) or fragility curves are developed for a bridge stock (wherein uncertainty is estimated on the basis of the analysis of the ‘typical’ bridge in each typological class), the proposed procedure for demand estimation is different, characterised by different level of accuracy and computational cost. In both cases demand is calculated in terms of displacement of the component control point.

- (a) *Single bridge analysis*: Nonlinear response history analysis using an enhanced IDA procedure proposed herein (IDA combined with Multiple Stripe Analysis [24]). Different suites of ground motions are selected at bedrock level for different ranges of earthquake intensity (each set is used for a small number of consecutive intensity levels). Inelastic soil behaviour may additionally be considered (whenever soil properties are known) using site response analysis to define ground motions at foundation surface. The equivalent cantilever height is estimated for all piers, while displacement demand is recorded at the control point of each component.
- (b) *Bridge stock analysis*: Response spectrum analysis is carried out using a simplified elastic model of the bridge for varying levels of earthquake intensity. Initial loading is based on the predominant mode pattern in each direction of the bridge (longitudinal, transverse) and the height of the equivalent cantilever (necessary for the calculation of component limit state thresholds) is estimated for each pier. Displacements developed at the control point of each critical component are recorded.
- (c) *Uncertainty demand - bridge stocks*: Bridges in the stock are divided into a number of typological classes; the scheme proposed in [4] is adopted here, wherein bridge classification is made according to pier type, deck type and pier-to-deck connection type. In the context of practical loss assessment for a road or railway network, uncertainty in demand ( $\beta_d$ ) is assumed to be the same for bridges classified in the same category. The  $\beta_d$  values are calculated for the representative bridge of each category (and each critical component) as described in (d).
- (d) For the specific bridge analysed or for the typical bridge in each class (see (c)), material, bearing, and soil properties, as well as gap size (of the deck joints or abutments), are considered as random variables (distribution, mean and dispersion values, as proposed in the literature). Bridge samples (typically  $N=100$ ) are generated assuming uncertainty in bridge modelling parameters, by means of Latin Hypercube sampling. Subsequently all bridge samples are paired with different earthquakes (typically 10, which, according to the enhanced IDA scheme described in (a), are not the same for all intensity levels); these are scaled to different PGA levels (0.1~1g), hence typically resulting in a total of 1000 analyses for the representative bridge of each typological class. Uncertainty in demand ( $\beta_d$ ) is calculated for each key component (piers, abutments, bearings).

*Step 3: Component and bridge system fragility*

- (a) *Bridge stock fragility*: An elastic response spectrum analysis of the simplified model is carried out for each bridge in the stock and for different PGA levels (typically for 0.1~1g, at 0.1g intervals). Results in terms of displacement ( $d$ ) demand at the control point of each critical component are plotted versus the earthquake parameter as depicted in Figure 2 (evolution of damage, or primary vulnerability, curve); PGA ( $A_g$ ) is used here, but other parameters, such as  $S_{pa}$  are also worth being explored. Capacity limit state thresholds are determined in terms of PGA (mean value), using the primary vulnerability curve and the definitions of damage in terms of  $d$ . Fragility curves for every limit state are then plotted assuming lognormal distribution:

$$P_f = \frac{1}{\sqrt{\beta_{tot}^2}} \cdot \ln \left( \frac{A_{g,m}}{A_{g,LS(i)}} \right) \quad (1)$$

The uncertainty  $\beta_{tot}$  is that derived in the previous steps for the typical bridge in the class to which the specific bridge belongs.

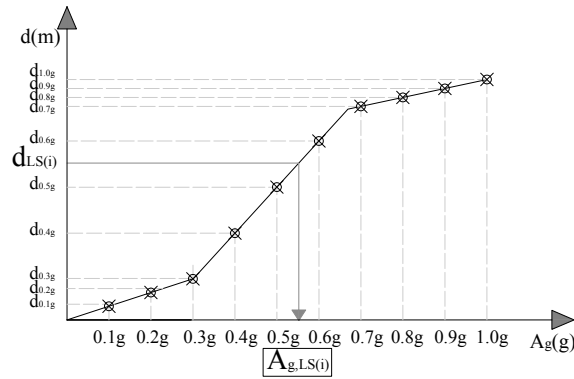


Figure 2. Evolution of damage (displacement demand versus earthquake parameter)

- (b) *Single bridge fragility*: The suite of inelastic response-history analyses (using the enhanced IDA procedure) for all bridge samples, earthquake motions and intensity levels have already been carried out in (d) of step 2; here the median displacement demand at the control point of every component is calculated, assuming lognormal distribution. Capacity limit state thresholds are defined in displacement terms for every bridge component (see Step1) and fragility curves are derived for every limit state considering the total uncertainty value, calculated for every component

$$P[D \geq C | IM] = \Phi \left( \frac{\ln(S_D/S_C)}{\sqrt{\beta_{tot}^2}} \right) \quad (2)$$

- (c) Assuming (conservatively) that the components form part of a series system for fragility evaluation, the damage threshold for the entire bridge is the lowest PGA value for any component. The exception to this is collapse; only piers or abutments are considered to control this limit state and in addition, unseating is also checked. Any degree of correlation between components can be considered. The degree of correlation is case-dependent and should be selected for every case separately, however the lower (full correlation) or upper (no correlation) bounds can be used for simplicity.

A flow chart of the methodology for the derivation of bridge specific fragility curves is shown in Figure 3.

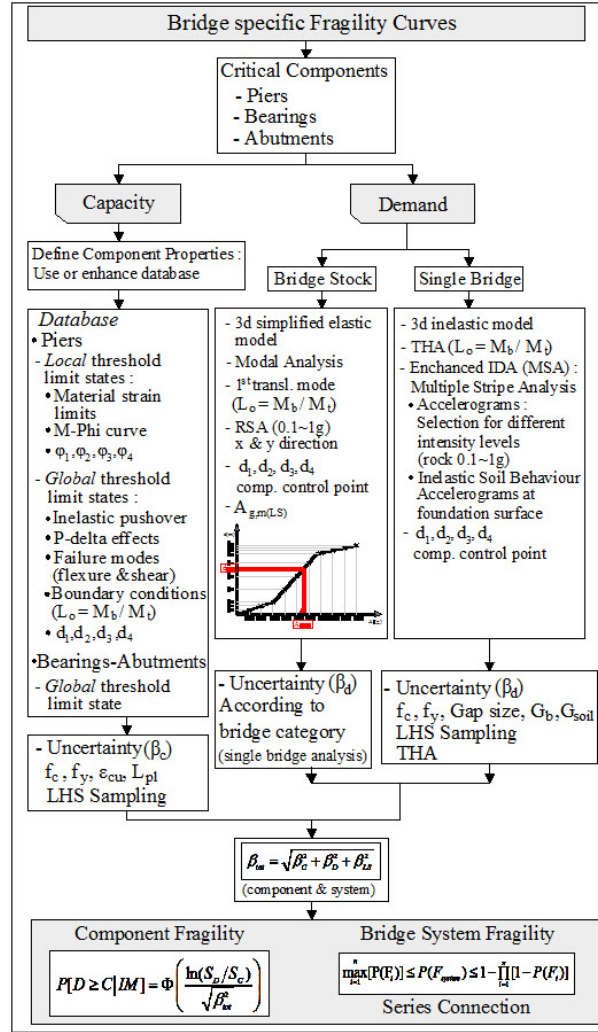


Figure 3. Flow chart for proposed methodology

### 2.1. Bridge Component Capacity and associated uncertainties

Different geometric, reinforcement, material and loading parameters affect the available strength and ductility, and eventually the seismic performance, of piers. It is noted that a cylindrical pier designed according to current code provisions (e.g. the Eurocodes) will eventually have a different limit state threshold (considered limit states are 1 to 4, see Table I) compared to a similar pier not having been designed according to code provisions (reinforcement ratio, confinement) or a pier with different axial load and, even more so, compared to a hollow rectangular or a wall-type pier. Therefore, a range of different characteristics (complying with code provisions, as well as substandard, in order to include older piers) is considered for every pier type; all plausible combinations of parameters are considered, hence creating a database that sufficiently describes bridge piers in the stock under consideration. Figure 4 shows a number of pier configurations representative of those commonly found in Southern Europe. Details of the range of parameters considered can be found in [25]; the longitudinal reinforcement ratio  $\rho_l$  ranges from 0.005 to 0.03, transverse reinforcement ratio  $\rho_w$  from 0.0025 to 0.015, concrete strength  $f_c$  from 16 to 35 (MPa), steel yield strength  $f_y$  from 220-500 (MPa) and normalised axial loading  $v_d$  axial loading  $v_d$  ( $N/(A_c f_{cd})$ , where  $A_c$  the section area and  $f_{cd}$  the design compressive strength of concrete) from 0.15 to 0.35.

Moment-curvature analysis is performed for all cross-sections included in the database using ad-hoc software [26] that incorporates stress-strain models for confined and unconfined concrete [27, 28], and for steel [29], producing a bilinear moment-curvature curve for each pier. Limit state thresholds are initially defined in curvature terms (local EDP) as depicted in Table I, related to the material strains developed.

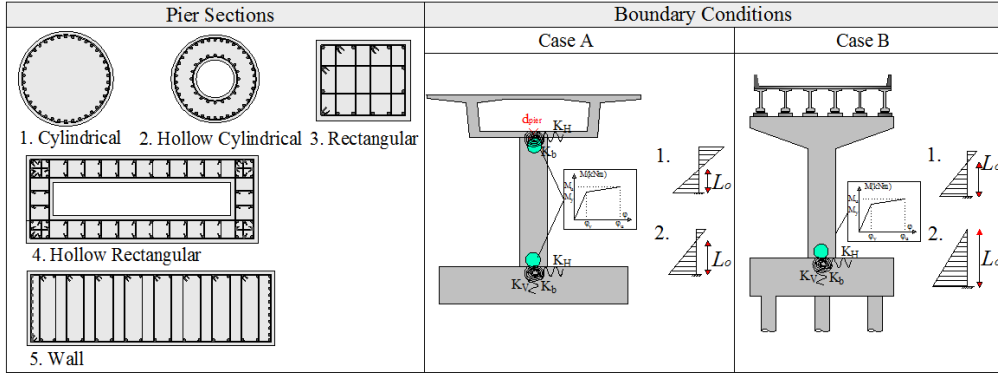


Figure 4. Pier types considered in the database and different boundary conditions

Table I. Component: Piers - Limit state definitions

Limit State (LS)	Threshold values of curvature ( $\varphi$ )	Quantitative Performance Description
LS 1 – Minor-Slight damage	$\varphi_1: \varphi_y$	Quasi-elastic behaviour – Cracks barely visible.
LS 2 – Moderate damage	$\varphi_2: \min(\varphi: \varepsilon_c > 0.004, \varphi: \varepsilon_s \geq 0.015)$	Spalling of the cover concrete; strength may continue to increase – Crack width 1-2mm.
LS 3 – Major-Extensive damage	$\varphi_3: \min(\varphi: \varepsilon_c \leq 0.004 + 1.4 \cdot \rho_w \cdot \frac{f_{yw}}{f_{cc}}, \varphi: \varepsilon_s \geq 0.06)$	First hoop fracture, buckling of longitudinal reinforcement, initiation of crushing of concrete core – Crack width > 2mm.
LS 4 – Failure-Collapse	$\varphi_4: \min(\varphi: M < 0.90 \cdot M_{max}, \varphi: \varepsilon_s \geq 0.075)$	Loss of load-carrying capacity - Collapse

Based on the results of moment-curvature analysis, empirical relationships for the estimation of the secant stiffness at yield ( $EI_{eff} = M_y / \varphi_y$ ) are derived for each pier type (as an example, equations 3 are empirical relationships for cylindrical piers).

$$\begin{aligned} \varphi_y &= \exp[-5.72 - 0.73 \cdot \ln(f_c / f_y) - 0.017 \cdot \ln(v_d) + 0.309 \cdot \ln \rho_l + 0.089 \cdot \ln \rho_w] \cdot D \\ M_y &= \exp[-0.37 - 0.63 \cdot \ln(f_c / f_y) + 0.22 \cdot \ln(v_d) + 0.55 \cdot \ln \rho_l + 0.053 \cdot \ln \rho_w] \cdot (2 \cdot \pi \cdot R^3 \cdot f_{cd}) \end{aligned} \quad (3)$$

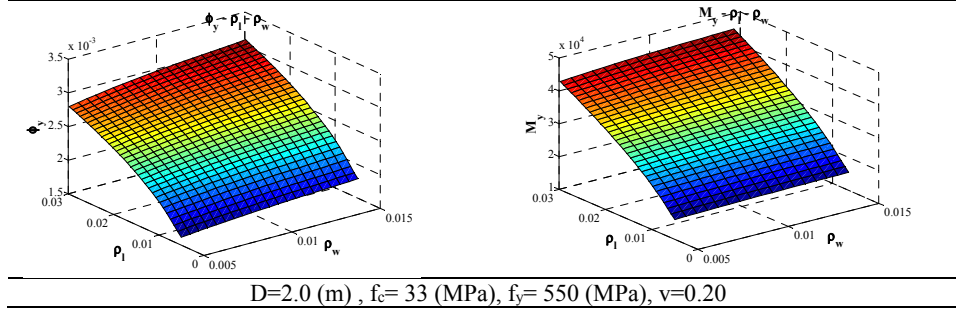


Figure 5. Yield moment and curvature of cylindrical section versus  $\rho_l$  and  $\rho_w$ .

The effect of longitudinal and transverse reinforcement ratio on yield moment and curvature of cylindrical sections is shown in Figure 5. Yield curvature, as well as yield and ultimate moment, are strongly affected by an increase in longitudinal reinforcement ratio, whereas an increase in transverse reinforcement mainly affects the ultimate curvature. Since  $\varphi_u$  is correlated with  $\varepsilon_{cu}$ , the ultimate curvature is strongly dependent on confinement of the core.

Pier sections are paired with different heights; a different height range is considered for each pier type, depicted in Figures 6 and 7, for the pier types shown in Fig. 4. The database should in principle include all pier types in the bridge stock analysed. Clearly, some lumping of similar types is necessary in real-life situations when large inventories are analysed (e.g. polygonal piers could be treated together with circular piers). Nonlinear static (pushover) analyses of the cantilever models are performed using appropriate software (here OpenSees [30]). For each pier type (and for both principal axes in non-symmetric cross-sections) from analysis that also considers P-delta effects, the displacement is recorded of the cantilever tip at the instant that the deformation of the plastic hinge exceeds limit state thresholds ( $\varphi_1, \varphi_2, \varphi_3, \varphi_4$  in Table 2); this is done using ad-hoc software developed in Matlab [31] for batch analysis. The relationship adopted for plastic hinge length estimation ( $L_{pl}$ ) affects the limit state thresholds calculated in displacement terms; therefore it should be carefully selected (here the relationships proposed in [32] and [33] have been used). Shear failure is also considered, since the shear demand at each step is compared with the ultimate shear capacity  $V_u$  [33], the associated displacement value is recorded and compared with the one derived considering flexural failure.

If all possible combinations of properties and pier heights are considered, a substantial number of pushover analyses results (as an example, 77760 analyses were carried out here for the case of hollow rectangular piers); from these analyses limit state thresholds in displacement terms ( $d_1, d_2, d_3, d_4$ ) are obtained. Analysis results are processed herein using the advanced least squares method (robust fit) and empirical relationships for threshold  $d_i$  values are provided for each pier type (equations 4 for the case of cylindrical piers, derived considering two different approximations for plastic hinge length estimation [32, 33]).

$$\begin{aligned}
 d_1 &= \exp[-6.52 - 0.88 \cdot \ln(D/H) - 0.02 \cdot \ln(v_d) - 0.69 \cdot \ln(f_c / f_y) + 0.09 \cdot \ln(\rho_w) + 0.29 \cdot \ln(\rho_l)] \cdot H \\
 d_2 &= \exp[-6.02 - 0.67 \cdot \ln(D/H) - 0.27 \cdot \ln(v_d) - 0.08 \cdot \ln(f_c / f_y) + 0.03 \cdot \ln(\rho_w) - 0.07 \cdot \ln(\rho_l)] \cdot H \\
 d_3 &= \exp[-3.87 - 0.57 \cdot \ln(D/H) - 0.24 \cdot \ln(v_d) - 0.47 \cdot \ln(f_c / f_y) + 0.50 \cdot \ln(\rho_w) - 0.11 \cdot \ln(\rho_l)] \cdot H \\
 d_4 &= \exp[-3.66 - 0.54 \cdot \ln(D/H) - 0.38 \cdot \ln(v_d) - 0.52 \cdot \ln(f_c / f_y) + 0.44 \cdot \ln(\rho_w) + 0.001 \cdot \ln(\rho_l)] \cdot H
 \end{aligned} \tag{4}$$

Use of equations like (4) increases the cost of analysis at the level of pier capacity determination but makes easier and more accurate the derivation of bridge-specific fragility curves, since there is no subsequent need for interpolation or simplification when piers of the bridges in the stock are analysed.

Capacity thresholds for the four limit states considered (Table I) are depicted in Figures 6 and 7 in terms of dimensionless global engineering demand parameters, namely displacement ductility ( $\mu_d$ ) and drift ( $d/h$ ). The variability in limit state thresholds, that depends on pier type and direction of loading, is evident; assuming a uniform value for the threshold may either overestimate or underestimate component capacity. It should be emphasised that Figures 6, 7 depict mean values, calculated by means of inelastic analysis of components included in the database, having a specific range of different parameters (different geometry, material, reinforcement ratio, and normalised axial load for each pier type).

From Figures 6 and 7, it is clear that hollow sections exhibit lower threshold values for all limit states considered (minor to collapse), compared to the relevant solid section values. For hollow circular piers and when displacement ductility is used as EDP, the latter observation is

due to the neutral axis depth that is greater than the tube thickness for the usual high axial loads ( $v_d > 0.15$ ) and reinforcement ratios, resulting in lower values of curvature ductility [34]. Since the results are dependent on the ultimate concrete strain value  $\epsilon_{cu}$  it should be further noted that different constitutive models for confined concrete are used for the case of circular [27] and rectangular [28] sections, which has an effect on the results.

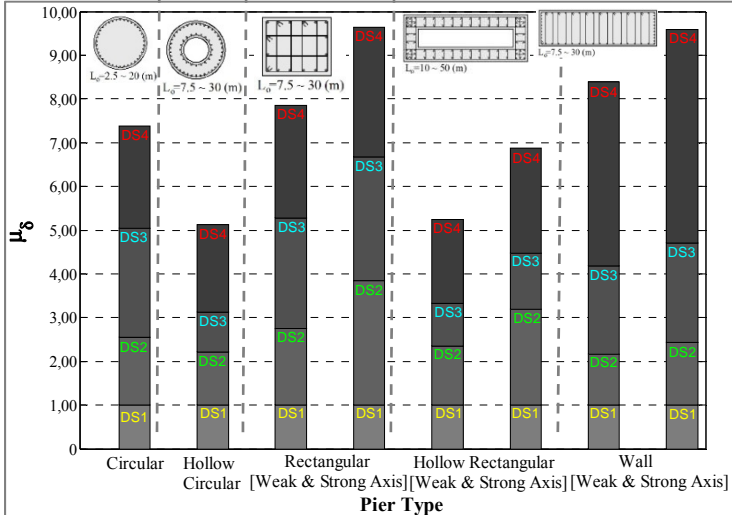


Figure 6. Displacement ductility for all limit states and pier types

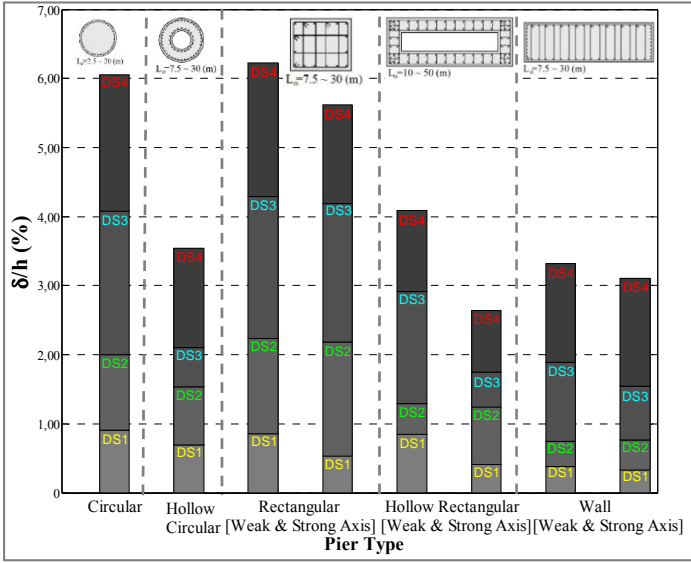


Figure 7. Drift values for all limit states and pier types

Regarding the hollow rectangular sections, it is noted that the curvature at yield is lower in their strong direction, resulting in higher curvature ductility (and eventually displacement ductility) than in the weak direction. When drift is used as an EDP, it is noted that limit state thresholds for hollow rectangular and wall sections are lower for all limit states considered. Global EDPs (related to pier displacement) are strongly dependent on the plastic hinge length, therefore the results may vary according to the selected relationship for the plastic hinge length [32].

Both experiment measurements and analysis results should be duly considered for all different pier types examined, to ensure consistency of the calculated capacity thresholds and verify the adequacy of the empirical relationships used for their calculation. Experimental tests on circular columns resulted in capacity thresholds for LS3 equal to 6.7 in terms of  $\mu_d$  and 6.5% in

terms of  $d/h$  [8]. Likewise,  $\mu_a$  values equal to 3.6 were recorded for the ultimate limit state (LS4) of hollow circular piers (compression-controlled section) [35], drift values equal to 7.8% for the ultimate limit state of rectangular sections [36],  $\mu_a$  values equal to 5.7 [37] and drift values equal to 3.14% [38] for the ultimate limit state of hollow rectangular piers, and drift values equal to 1.5% for wall piers (LS3) [39]. These values are in agreement with the calculated threshold capacity values in terms of  $\mu_a$  and drift presented in Figures 6 and 7.

Depending on the boundary conditions, i.e. the type of pier to deck connection and the type of foundation and supporting ground, the pier bending moment diagram varies, as shown in Figure 8. Foundation flexibility is ignored in bridge stock analysis, which is a reasonable assumption for relatively stiff ground types (A and B in Eurocode 8). However, boundary conditions at pier top are considered; they vary according to deck properties and pier-to-deck connection (rotational springs, case C - Figure 8). Therefore the equivalent cantilever height  $L_o$ , corresponding to the level of the contraflexure point, should be estimated in order to use the proposed empirical relationships, derived from pushover analyses of a cantilever. Limit state thresholds ( $d_1, d_2, d_3, d_4$ ), calculated for the equivalent cantilever height ( $L_o$ ), should be subsequently correlated to top displacement of the restrained pier. All possible cases are shown in Figure 8; note that Cases A and B are the theoretical limits, case A is not applicable if the deck is a box girder, and case D is not addressed herein since foundation compliance is ignored.

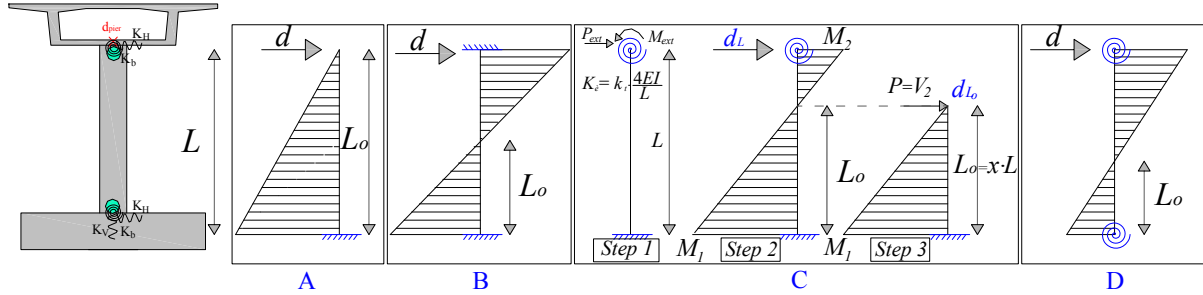


Figure 8. Location of contraflexure point for different boundary conditions

For relating the equivalent cantilever length to the displacement at the top of the pier, the three steps described in Figure 8 are applied. In the general case of the restrained pier (Step 1 – Figure 8), equation (5) expresses equilibrium, using the reduced (including boundary conditions) stiffness matrix of the structure.

$$\begin{bmatrix} P_{ext} \\ M_{ext} \end{bmatrix} = \begin{bmatrix} \frac{12EI}{L^3} & -\frac{6EI}{L^2} \\ -\frac{6EI}{L^2} & \frac{4EI}{L} + \left[ \frac{4EI}{L} \cdot k_t \right] \end{bmatrix} \cdot \begin{bmatrix} d_{(L)} \\ \theta_{(L)} \end{bmatrix} \quad (5)$$

Displacement  $d_L$  is imposed at the top of the restrained pier (Step 2 – Figure 8). According to equation (5), the top rotation ( $\theta_L$ ) of the restrained pier is related to the top displacement ( $d_L$ ) (equation 6):

$$\theta_{(L)} = \frac{6EI/L^2}{\left( \frac{4EI}{L} \right) \cdot (1 + k_t)} \cdot d_{(L)} \quad (6)$$

Therefore, using the elastic beam stiffness matrix and replacing  $\theta_L$ , the internal shears and moments are expressed as:

$$\begin{aligned}
V_1 = V_2 &= \frac{12EI(0.25 + k_t)}{L^3 \cdot (1 + k_t)} \cdot d_{(L)} \\
M_1 &= \frac{6EI(0.5 + k_t)}{L^2 \cdot (1 + k_t)} \cdot d_{(L)}, \quad M_2 = \frac{6EI(-k_t)}{L^2 \cdot (1 + k_t)} \cdot d_{(L)}
\end{aligned} \tag{7}$$

Based on the above, the equivalent cantilever height ( $L_o$ ) is calculated (equation 8):

$$\frac{L_o}{L} = \frac{M_1}{M_1 + M_2} = \frac{(0.5 + k_t)}{2 \cdot (0.25 + k_t)} \tag{8}$$

Finally (Step 3 – Figure 8), the top displacement ( $d_{L_o}$ ) of the equivalent cantilever having height  $L_o$ , is related to the top displacement of the restrained pier ( $d_L$ ). External force  $V_2$  is applied, since base moment should be equal in both pier cases (restrained pier of Step 2 and equivalent cantilever of Step 3 – Figure 8, equation 9) :

$$\begin{bmatrix} \frac{12EI}{L^3} & -\frac{6EI}{L^2} \\ -\frac{6EI}{L^2} & \frac{4EI}{L} \end{bmatrix} \cdot \begin{bmatrix} d_{(L_o)} \\ \theta_{(L_o)} \end{bmatrix} = \begin{bmatrix} V_{ext} (= V_2) \\ M_{ext} (= 0) \end{bmatrix} \tag{9} \quad , \quad d_{(L)} = \left( \frac{6x-2}{4 \cdot x^3} \right) \cdot d_{(L_o)} \tag{10}$$

The limit state thresholds of a restrained pier (height  $L$ ) can be obtained from equation (10), in terms of the relevant values of the equivalent cantilever (height  $L_o$ ); term  $x$  is further explained in Figure 8 (Case C). It should be mentioned at this point, that the above relationships are strictly valid for an elastic pier; however, on the basis of the equal displacement approximation (valid for  $T > T_c$ , where  $T_c$  is the corner period of the design response spectrum, which is the case for the majority of bridges) equation (10) can be used for a reasonable prediction of the inelastic displacements as well. Finally it should be mentioned that equation (10) is also applicable to multicolumn piers, provided that  $L_o$  is defined for each pier, under the assumption that failure in the cap beam or the joints is prevented.

Limit state definitions for the **abutments** are given in Table II (based on [9]). Inelastic static (pushover) analysis is performed for the abutment subsystem (Figure 9) in order to define the threshold value in terms of displacement of the control point for the first limit state. The other three states are directly expressed in terms of fractions of the backwall height, based on recommendations from the literature, also adopted by Caltrans. Threshold values are related to experimentally observed soil damage, whereas a trilinear relationship between initial stiffness and ultimate deformation is assumed to model nonlinear passive action.

The local EDP used to define limit state thresholds for elastomeric **bearings** is the shear strain ( $\gamma = d/t_r$ , where  $t_r$  is the thickness of the elastomer). Threshold values based on information from the literature [4, 6, 9] are given in Table III. For the first limit state the conservative value proposed in [4] is adopted, since the displacement for the proposed shear strain is approximately equal to the yield displacement of the bearing as proposed in [40]. For the ultimate limit state threshold, a strain of 300% is proposed, and an additional check is made that the critical buckling load [40] is not exceeded. In general, test results are used to relate the local EDP to experimentally observed damage (yield of shims, uplift, etc.).

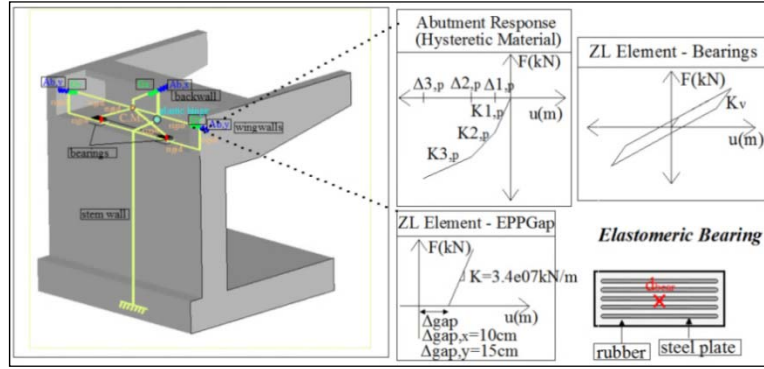


Figure 9. Components: Abutments and bearings - Limit state thresholds in displacement terms

Table II: Component Abutments: Limit state thresholds (global EDP)

Limit State	Threshold values	Quantitative Performance Description
LS 1 – Minor/Slight damage	$d = 1.1 \cdot d_{gap}$ $(\mu_{\phi,backwall} = 1.5)$	Cracking and significant damage to the backwall
LS 2 – Moderate damage	$d = 0.01 \cdot h_{backwall}$	First yield of the abutment soil
LS 3 – Major/Extensive damage	$d = 0.035 \cdot h_{backwall}$	Excessive deformation of abutment soil
LS 4 – Failure/Collapse	$d = (0.1 \sim 0.06) \cdot h_{backwall}$	Ultimate deformation of abutment soil (cohesive~cohesionless soil)

Table III: Component Bearings: Limit state thresholds (global EDP)

Limit State	Threshold ( $\gamma$ ) values	Quantitative Performance Description
LS 1 – Minor/Slight damage	20%	Initiation of nonlinear behaviour (yielding displacement of piers), potential yielding of anchor bolts and cracking of pedestals.
LS 2 – Moderate damage	100%	Visible damage to the bearing; yield of steel shims.
LS 3 – Major/Extensive damage	200%	Lift off at the edge of the bearing, uplift and rocking; may cause delamination, bonding failure between rubber layers and steel shim plates.
LS 4 – Failure/Collapse	300%	Lift-off, rotation; unseating, failure of bearings.

### Uncertainty analysis

Uncertainty in capacity ( $\beta_c$ ) is considered, assuming the distribution of key random variables, namely material strengths, ultimate concrete strain and plastic hinge length, with mean and standard deviation values as shown in Table IV, according to [9], [41]; the other parameters were treated as deterministic. Latin Hypercube sampling is used to generate N statistically different, yet nominally identical, pier samples (N=100) for two different pier heights, representative of tall and short piers. Analysis results were processed and  $\beta_c$  values are proposed for each pier type and limit state in Table V. Based on the  $\beta_c$  values presented in Table V, and noting that the average  $\beta_c$  for all limit states varies from 0.31 to 0.41, if a uniform value for the uncertainty in pier capacity is sought, this could be taken equal to 0.35.

Table IV: Assumed distributions for random variables (uncertainty in pier capacity)

Random Variable	Distribution	Mean	COV
$f_c$ (MPa)	normal	34.5	18%
$f_y$ (MPa)	normal	463	8%
$\varepsilon_{cu}/\varepsilon_{cu,model}$ (%)	normal	0.99	35.8%
$L_{pl}/L_{pl,model}$	uniform	0.96	47.4%

Uncertainty in limit state definition ( $\beta_{LS}$ ) is quantified considering the range of limit state threshold values proposed in the literature for different EDPs, and calculating the dispersion, assuming lognormal distribution.

Table V: Uncertainty in capacity ( $\beta_c$ ) for various pier types

Pier Type	$\beta_{c, LS1}$	$\beta_{c, LS2}$	$\beta_{c, LS3}$	$\beta_{c, LS4}$	$\beta_{c, LS1-4}$
Cylindrical	0.14	0.36	0.48	0.49	<b>0.37</b>
Hollow Cylindrical	0.10	0.15	0.48	0.55	<b>0.32</b>
Rectangular (strong direction)	0.14	0.20	0.40	0.48	<b>0.31</b>
Rectangular (weak direction)	0.14	0.32	0.42	0.48	<b>0.34</b>
Hollow Rectangular (strong direction)	0.22	0.32	0.40	0.41	<b>0.34</b>
Hollow Rectangular (weak direction)	0.22	0.36	0.42	0.43	<b>0.36</b>
Wall (strong direction)	0.16	0.29	0.43	0.48	<b>0.34</b>
Wall (weak direction)	0.23	0.33	0.40	0.50	<b>0.41</b>

The range of limit state thresholds proposed in the literature for bridge piers, in terms of different EDPs, namely pier drift ( $d/H\%$ ), displacement ductility ( $\mu_d$ ), rotation ductility ( $\mu_\theta$ ) and curvature ductility ( $\mu_\phi$ ), is depicted in Figure 10. It was found that despite the fact that a greater logarithmic dispersion value ( $\beta_{LS}$ ) would be expected for higher limit states, this is not the case for all EDPs; for example in the case of ultimate drift, the dispersion is equal to zero. Uncertainty in limit state definition is quantified for all limit states and EDPs considered, see Table VI. Consideration of a uniform  $\beta_{LS}$  value equal to 0.35 is, in general, a reasonable choice; bearing in mind the aforementioned inconsistency regarding the higher limit states,  $\beta_{LS} = 0.35$  is proposed for the definition of LS in the case of pier capacity.

Table VI: Uncertainty in limit state definition ( $\beta_{LS}$ ) for different engineering demand parameters

EDP (for piers)	$\beta_{LS}$			
	LS1	LS2	LS3	LS4
Drift (%)	0.34	0.41	0.12	0.00
$\mu_\delta$	0.44	0.39	0.46	0.27
$\mu_\theta$	0.31	0.34	0.21	0.57
$\mu_\phi$	0.63	0.57	0.63	0.53
$\beta_{LS,mean}$	<b>0.43</b>	<b>0.43</b>	<b>0.36</b>	<b>0.34</b>

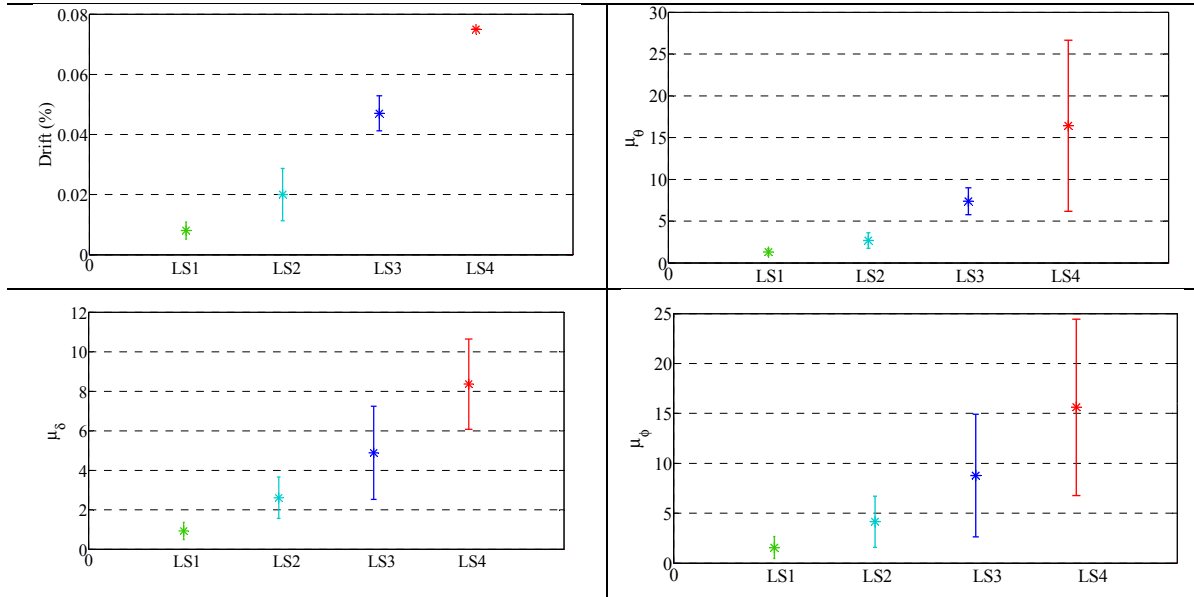


Figure 10. Range of limit state thresholds proposed in literature for piers (drift,  $\mu_\theta$ ,  $\mu_\delta$ ,  $\mu_\phi$ )

The range of limit state thresholds proposed in the literature for bearings and abutments is depicted in Figure 11. The dispersion is apparently greater for higher limit states, while a uniform  $\beta_{LS}$  value equal to 0.20 and 0.47 is proposed the case of bearings and abutments, respectively.

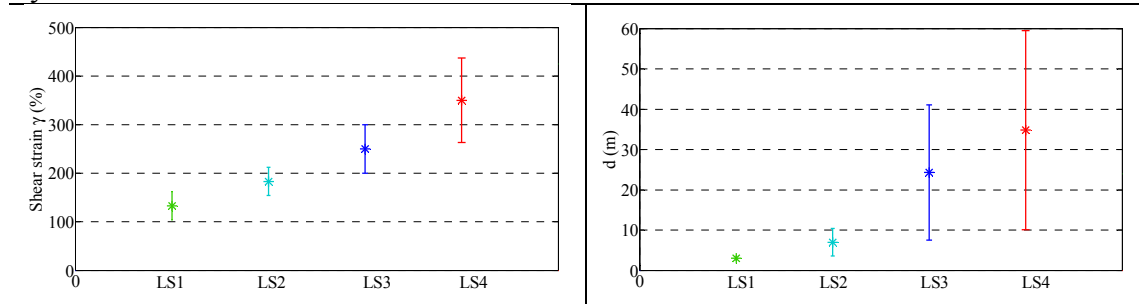


Figure 11. Range of limit state thresholds values proposed in literature for bearings (left) and abutments

Epistemic uncertainties arising from modelling assumptions and software used for the analysis, are not explicitly defined at this stage of development of the methodology. Therefore they can be considered in a simplified manner ( $\beta_u=0.20$ ) as proposed in [21], or quantified according to the methodology proposed in [16].

## 2.2. Bridge component seismic demand and associated uncertainties

Seismic demand is calculated at the control point of every critical component based on the results of response-history analysis of a detailed inelastic model (single bridge case) or response spectrum analysis of simplified elastic model (bridge stock case) for varying levels of earthquake intensity (Step 2). In nonlinear response-history analysis of the inelastic model, statistically different yet nominally identical bridge samples are analysed (N=100) and the enhanced IDA procedure is applied. The random variables considered, having distributions and COV values as proposed in the literature [41, 42, 14] and mean values according to the properties of a typical bridge studied [25], are presented in Table VII. Every bridge realization is paired (according to [43]), with selected earthquake ground motions (10 different motions for 10 earthquake levels), resulting in a total of 1000 analyses.

Table VII: Assumed distributions for random variables (uncertainty in demand) in a typical bridge

Random Variable	Distribution	Mean	COV
$f_c$	normal	28 MPa	18%
$f_y$	normal	506 MPa	8%
gap size	normal	20 cm	20%
bearings	uniform	$G=0.9$ MPa	22%
soil properties	uniform	$G=660$ MPa	20%

Regarding the ground motion selection, the 1<sup>st</sup> edition of the PEER NGA record database is used. A suite of 10 individual ground motions for each level of intensity (PGA from 0.1g to 0.4g, 0.5g to 0.7g, 0.8 to 1g, scaled at 0.1g steps) is selected at bedrock [44], using the Eurocode 8 elastic spectrum as target spectrum (Figure 12). Different suites of ground motions are selected at bedrock level for various levels of earthquake intensity; appropriate division of the intensity levels into three groups is considered (Multiple Stripe Analysis [24]), assuming different initial constraints for magnitude (M) and epicentral distance (R) in every group (here, group 1:  $M < 6.5$ , group 2:  $M \geq 6.5$ ,  $R > 30$ , group 3:  $M \geq 6.5$ ,  $R < 30$ ). Inelastic soil behaviour may additionally be considered as described in (c) of Step 2 and Figure 12.

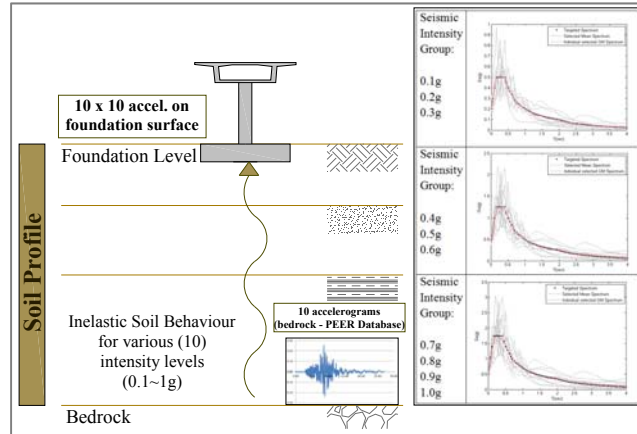


Figure 12. Selection of ground motion suites for different intensity measures (Multiple Stripe Analysis)

The quantification of uncertainties in seismic demand ( $\beta_d$ ) for bridge components is highly dependent on the selection of earthquake motions, the earthquake intensity, bridge geometry and structural system, as well as component properties. In the proposed methodology, classification of bridges is made according to the scheme described in [4]; analysis of a representative bridge in each category is considered sufficient for bridge stock fragility analysis, wherein a uniform value for all bridges that fall within the same category is assumed (for each component). Response-history analyses for the suite of earthquake ground motions for different intensity levels are performed and uncertainty in demand is calculated for each component.

As an example, uncertainty in seismic demand of critical components ( $\beta_d$ ) is calculated for a simply-supported case study bridge (Figure 13, representative of #232 category [4], i.e. rectangular hollow piers, deck consisting of simply-supported precast-prestressed beams, bearing-supported on the piers) according to the proposed methodology, as depicted in Table VIII. It is clear that  $\beta_d$  values vary among different components (maximum value for piers, minimum for abutments), and in general increase for higher levels of earthquake intensity. It appears that uncertainty in seismic demand may be equal, greater, or even less than the commonly adopted HAZUS value ( $\beta_d=0.50$ , [21]). In line with the above, a uniform, but different for each critical component, value (average of all intensities) is recommended in a practical context (last column

of Table VIII). Different  $\beta_d$  values have been estimated for different bridge categories; values are similar among bridges with monolithic pier-to-deck connections, and also among bridges with bearing-supported decks.

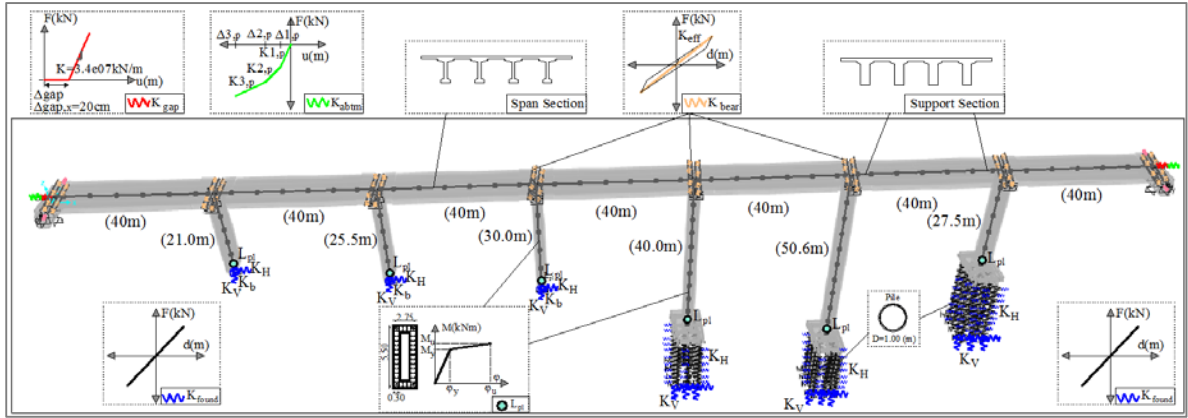


Figure 13. Case Study of representative bridge of type ‘simply-supported prestressed beams’

Table VIII: Uncertainty in component demand ( $\beta_d$ ): bridges ‘with simply-supported prestressed beams

Longitudinal Direction											
Component	$\beta_d$ (0.1g)	$\beta_d$ (0.2g)	$\beta_d$ (0.3g)	$\beta_d$ (0.4g)	$\beta_d$ (0.5g)	$\beta_d$ (0.6g)	$\beta_d$ (0.7g)	$\beta_d$ (0.8g)	$\beta_d$ (0.9g)	$\beta_d$ (1.0g)	$\beta_d$
Piers	0.45	0.44	0.46	0.82	0.81	0.81	0.85	0.89	0.87	0.86	<b>0.73</b>
Bearings	0.37	0.41	0.43	0.84	0.86	0.85	0.84	0.83	0.82	0.81	<b>0.71</b>
Abutments	--	--	0.25	0.28	0.30	0.48	0.55	0.83	0.83	0.82	<b>0.51</b>
Transverse Direction											
Component	$\beta_d$ (0.1g)	$\beta_d$ (0.2g)	$\beta_d$ (0.3g)	$\beta_d$ (0.4g)	$\beta_d$ (0.5g)	$\beta_d$ (0.6g)	$\beta_d$ (0.7g)	$\beta_d$ (0.8g)	$\beta_d$ (0.9g)	$\beta_d$ (1.0g)	$\beta_d$
Piers	0.45	0.44	0.45	0.82	0.80	0.79	0.84	0.82	0.80	0.85	<b>0.71</b>
Bearings	0.44	0.42	0.42	0.84	0.85	0.84	0.79	0.78	0.77	0.77	<b>0.69</b>
Abutments	0.16	0.15	0.18	0.49	0.49	0.49	0.46	0.45	0.44	0.46	<b>0.38</b>

### 2.3. Bridge system fragility

Bridge-specific fragility curves can be generated according to Step 3 of the proposed methodology ((b) or (c) according to the problem at hand), based on component fragility, since both capacity and demand have been explicitly defined for each critical component. The total uncertainty value is calculated at component level according to equation 11, under the assumption of statistical independence.

$$\beta_{tot} = \sqrt{\beta_C^2 + \beta_D^2 + \beta_{LS}^2} \quad (11)$$

The estimation of total uncertainty at system level is related to the structural system of the bridge; it is governed by pier (total) uncertainty for the case of monolithic bridge to deck connection, by bearings in simply supported bridges, and by abutments in single-span bridges. The same total uncertainty value is also used when seismic demand is estimated on the basis of elastic response spectrum analysis of the simplified model (bridge stock analysis), to approximately account for uncertainty due to inelastic behaviour and ground motion variability.

Series connection between components is conservatively assumed for the derivation of bridge fragility curves, according to equation 12 (upper and lower bounds). The results presented herein are for the lower bound (completely correlated components), however the exact system fragility lies within these two bounds and depends on the component correlation level that can be calculated for each individual bridge.

$$\max_{i=1}^n [P(F_i)] \leq P(F_{system}) \leq 1 - \prod_{i=1}^{\pi} [1 - P(F_i)] \quad (12)$$

Since collapse of the bridge system is not expected to occur if just the bearings reach LS4, limit state 4 at bridge (as a system) level is related to pier or abutment failure only. Therefore the series connection assumption is not invoked for the estimation of system fragility for the ‘collapse’ limit state.

### 3. DEVELOPMENT OF TOOLS FOR FRAGILITY ANALYSIS

As should be clear from the previous section, substantial amount of analytical work is inevitably required if bridge-specific fragility curves are sought; hence analysis tools (additional to the software for carrying out the dynamic analysis of the bridge models) are indispensable, particularly when bridge stocks are analysed. For this case, a Matlab-based software was developed for the implementation of the previously described methodology using the simplified elastic model and response spectrum analysis for the derivation of bridge-specific fragility curves, summarised in Figure 14. The software is based on a generic simplified 3D bridge model created using the OpenSees platform [30]. Input data provided by the user are depicted in Figure 14 and include general bridge geometry, (non-seismic) loading, component properties (piers, bearings, abutments), and the pertinent response spectrum. Limit state thresholds for piers are automatically calculated according to the properties and boundary conditions of the specific bridge analysed, while dispersion (uncertainty) values are also calculated following the previously described procedure. Different boundary conditions at abutments are considered for the case of open and closed gap; fragility curves are automatically calculated for the longitudinal and transverse directions separately, using the former model analysis results up to gap closure (Figure 14).

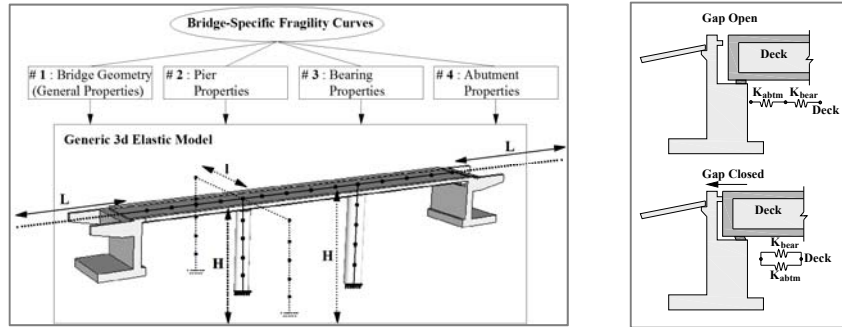


Figure 14. Generic 3D bridge model and abutment boundary conditions before and after gap closure

The developed software drastically reduces the time and effort required for the implementation of the proposed methodology to a large number of bridges within an inventory. The methodology has been applied (as a pilot study) to the bridge stock of the Western Macedonia (Greece) section of Egnatia Motorway, as part of the seismic loss assessment of this road network. The fragility curve derivation module has been included in a GIS-based software for the management of seismic risk of road networks.

### 4. EXAMPLES OF BRIDGE-SPECIFIC FRAGILITY CURVES

Fragility curves for a simply-supported bridge, shown in Figure 13, representative of category 232 (see section 2.2) were calculated at system level using the methodology described herein, under the assumption of series connection between components (disregarding bearings in LS4). The curves of Figure 15 correspond to the lower bound of equation 12 for the system fragility estimation, while the difference in the thresholds (%) in case that the upper bound is

used (mean value for each LS) is also depicted in the legend; consistently with previous findings in the literature (e.g. [5]), the differences are smaller in the lower damage states. Both sets of fragility curves derived using inelastic response-history analysis of the detailed inelastic model for the demand estimation (IDA-MSA), and elastic analysis results (RSA) of the simplified model (using the software developed) and the uncertainty values proposed herein (Table VIII), are shown in Figure 15. It appears that approximate elastic analysis of the demand can lead to a reasonable (usually slightly conservative) estimation of the probability of damage of the bridge system for limit states 1 to 3 (taking IDA-MSA as the benchmark), whereas elastic analysis may result in non-conservative results for limit state 4, attributed basically to the nonlinear behaviour of piers.

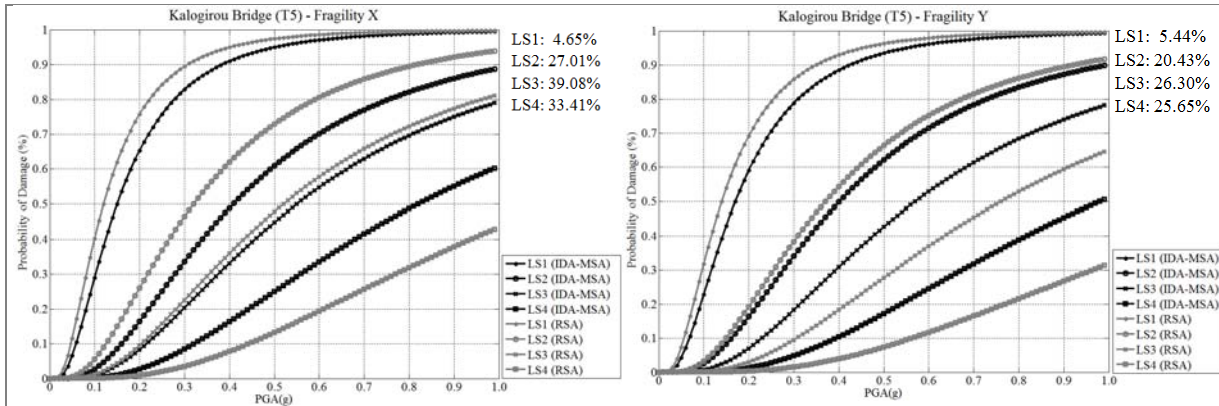


Figure 15. Fragility curves of case study bridge (T5) in longitudinal and transverse direction (IDA and RSA)

## 5. FINAL REMARKS AND CONCLUSIONS

The study presented herein aims at incorporating research on component capacity and demand and the associated uncertainties into a methodology for the derivation of bridge-specific fragility curves for different limit states. Procedures of different complexity and computational cost are adopted depending on whether a single bridge or an entire bridge stock is assessed; nonetheless, the derived fragility curves are bridge specific in either case, but inevitably the level of accuracy is higher in the former case. A key idea in this endeavour is that the fragility curves are readily derived for each individual bridge by extracting damage threshold values and the associated uncertainties for each component from a database of critical components. Clearly, it is impossible to compile a database encompassing all usual types of bridges within a single study; nevertheless the database presented herein may be used for a large number of bridges, with special focus on typologies commonly found in seismic-prone areas of Europe. It is envisaged that this bridge component fragility database will soon be made available on-line, along with the associated analysis tools; international users will be encouraged to carry out their own analyses and contribute additional pier, abutment and bearing fragility data to this open database. Additional work is worth carrying out regarding the definition of limit state thresholds for abutments, using advanced models including both the abutment per se and the backfill system.

The most important findings from the application of the methodology to a specific bridge stock (in Southern Europe) are summarised in the following.

- All critical components should be considered for the derivation of bridge fragility curves. In addition to those addressed herein (piers, abutments, bearings), one could also consider foundation elements that might be critical in some bridge types (e.g. failure of piles supporting the abutments).

- Limit state thresholds of components should be expressed in terms of global EDPs (typically displacements) and be correlated to local damage. Component-specific limit state thresholds should be explicitly defined considering different type, geometry, material, reinforcement ratios, loading properties, and boundary conditions; all these affect component capacity and relevant threshold values.
- Uncertainty in capacity, demand, and limit state definition should be considered for each component and limit state separately; a total uncertainty value appropriate for the specific structural system should then be calculated.
- Bridge-specific fragility curves should be based on explicit estimation of bridge component capacity and demand, as opposed to adopting uniform fragility values for bridges that fall within the same category according to a classification scheme; the latter is currently done for bridge and road network loss assessment studies.
- To improve the reliability of fragility assessment, when inelastic response-history analysis (IDA) is used for demand estimation, selection of different suites of ground motions for different ranges of earthquake intensity level (MSA) is in order.
- When elastic (RSA) analysis is used for demand estimation, a simplified 3D model can be used, in preference to the, admittedly less demanding, equivalent single-degree-of-freedom model. This allows to account for the correlation between different components and the dependence of the displacement profile on deck geometric properties and boundary conditions.
- Elastic analysis of the demand for the simplified model seems to work well for the first three damage states, but to underestimate fragility for the ‘collapse’ limit state.

#### ACKNOWLEDGEMENTS

This research has been co-financed by the European Union (European Social Fund – ESF) and Greek national funds through the Operational Programme “Education and Lifelong Learning” of the National Strategic Reference Framework (NSRF) – Research Funding Program: *ARISTEIA II: Reinforcement of the interdisciplinary and/or interinstitutional research and innovation*. The authors would like to thank Prof. Anastasios Sextos and PhD Candidate N. Lesgidis for the selection of the accelerograms, Egnatia Odos S.A. for providing the data of the case study bridges, and all participants to the RETIS-Risk research programme for their cooperation in this multi-disciplinary project.

#### REFERENCES

1. Billah AHMM, Alam MS. Seismic fragility assessment of highway bridges: a state-of-the-art review. *Structure and Infrastructure Engineering* 2015; **11**(6):804-832.
2. Cardone D. Displacement limits and performance displacement profiles in support of direct displacement-based seismic assessment of bridges. *Earthquake Engineering & Structural Dynamics* 2013; **43**(8):1239-1263.
3. Banerjee S, Shinozuka M. Nonlinear Static Procedure for Seismic Vulnerability Assessment of Bridges. *Computer-Aided Civil and Infrastructure Engineering* 2007; **22**(4):293–305.
4. Moschonas IF, Kappos AJ, Panetsos P, Papadopoulos V, Makarios T, Thanopoulos P. Seismic fragility curves for greek bridges: methodology and case studies. *Bulletin of Earthquake Engineering* 2008; **7**(2):439–468.
5. Choi E, DesRoches R, Nielson B. Seismic fragility of typical bridges in moderate seismic zones. *Engineering Structures* 2004; **26**(2):187–199.

6. Zhang J, Huo Y. Evaluating effectiveness and optimum design of isolation devices for highway bridges using the fragility function method. *Engineering Structures* 2009; **31**(8):1648–1660.
7. DesRoches R, Padgett J, Ramanathan K, Dukes J. Feasibility Studies for Improving Caltrans Bridge Fragility Relationships. Report CA 12-1775. Georgia Institute of Technology, Atlanta, U.S.A, 2012.
8. Berry M, Eberhard M. *Performance Models for Flexural Damage in Reinforced Concrete Columns*. PEER Report 2003/18, University of California, Berkeley, 2003.
9. Nielson BG. Analytical Fragility Curves for Highway Bridges in Moderate Seismic Zones Analytical Fragility Curves for Highway Bridges in Moderate Seismic Zones. *PhD Thesis*, Georgia Institute of Technology, Atlanta, 2005.
10. Crowley H, Colombi M, Silva V, Monteiro R, Ozcebe S, Fardis M, Tsionis G, Askouni P. *SYNER-G : Deliverable D3.6-Fragility functions for roadway bridges*, University of Pavia, Italy, 2011.
11. Hwang H, Jernigan JB, Lin Y-W. Evaluation of Seismic Damage to Memphis Bridges and Highway Systems. *Journal of Bridge Engineering*, (ASCE) 2000; **5**(4):322–330.
12. Fajfar, P. Capacity Spectrum Method Based on Inelastic Demand Spectra. *Earthquake Engineering & Structural Dynamics* 1999; **28**(9):979–993.
13. Shinozuka M, Feng MQ, Kim H, Kim S-H. Nonlinear Static Procedure for Fragility Curve Development. *Journal of Engineering Mechanics (ASCE)* 2000; **126**(12):1287–1295.
14. Elnashai AS, Borzi B, Vlachos S. Deformation-based vulnerability functions for RC bridges. *Structural Engineering and Mechanics* 2004; **17**(2):215–244. Kircher C, Nassar A, Kustu O, Holmes W. Development of buildings earthquake loss damage functions for earthquake loss estimation. *Earthquake Spectra* 1997; **13**(4):663–682.
15. Mackie KR, Nielson, BG. Uncertainty Quantification in Analytical Bridge Fragility Curves. *Proc. of TCLEE :Lifeline Earthquake Engineering in a Multihazard Environment (ASCE)*, Oakland, California, 2009.
16. Aviram A, Mackie K, Stojadinovic, B. Epistemic Uncertainty of Seismic Response Estimates for Reinforced Concrete Bridges. *Proc. of 14th World Conference of Earthquake Engineering*. Beijing, China, 2008.
17. Towashiraporn, P. Building Seismic Fragilities using Response Surface Metamodels. *PhD Thesis*, Georgia Institute of Technology, 2004.
18. Shinozuka M, Feng MQ, Lee J, Naganuma T. Statistical Analysis of Fragility Curves. *Journal of Engineering Mechanics (ASCE)*, 2000; **126**(12):1224–1231.
19. Padgett JE, Nielson BG, DesRoches R. Selection of optimal intensity measures in probabilistic seismic demand models of highway bridge portfolios. *Earthquake Engineering and Structural Dynamics*, 2008; **37**:711–725.
20. Mander J, Basöz N. Enhancement of the Highway Transportation Lifeline Module in HAZUS. Final Pre-Publication Draft (#7) prepared for the National Institute of Building Sciences (NIBS), 1999.
21. Kappos A, Sextos A, Stefanidou S, Mylonakis G, Pitsiava M, Sergiadis G. (2014). Seismic Risk of Inter-Urban Transportation Networks. *Procedia-Economics & Finance* 2014; **18**:263 – 270
22. Iman RL, Conover WJ. A distribution-free approach to inducing rank correlation among input variables. *Communications in Statistics-Simulation and Computation*, 2007; **11**(3):311–334.
23. Baker JW. Trade-offs in ground motion selection techniques for collapse assessment of structures. *Proc. of Vienna Congress on Recent Advances in Earthquake Engineering and Structural Dynamics*, Vienna, Austria, 2013, paper no. 123.

24. Stefanidou S. Bridge Specific Fragility Curves for As Built and Retrofitted Bridges, *PhD. Thesis (in greek)*. Aristotle University of Thessaloniki, Greece, 2015.
25. Papanikolaou VK. Analysis of arbitrary composite sections in biaxial bending and axial load. *Computers and Structures* 2012; **98-99**:33–54.
26. Mander JB, Priestley MJN, Park R. Theoretical Stress-Strain Model for Confined Concrete. *Journal of Structural Engineering* 1988; **114**(8):1804-1826.
27. Kappos AJ. Analytical Prediction of the Collapse earthquake for R/C buildings: Suggested Methodology. *Earthquake Engineering & Structural Dynamics* 1991; **20**:167–176.
28. Park R, Sampson RA. Ductility of Reinforced Concrete Column Sections in Seismic Design. *ACI Journal Proceedings* 1972; **69**(9):543-555.
29. McKeena F, Fenves GL. *Open System for Earthquake Engineering Simulation*. Pacific Earthquake Engineering Research Center, 2015.
30. Mathworks. *Matlab: Language of Technical Computing*. New York: Mathworks, 2011.
31. Biskinis D, Fardis MN. Flexure-controlled ultimate deformations of members with continuous or lap-spliced bars. *Structural Concrete* 2010; **11**(2):93-108.
32. Priestley MJN, Calvi GM, Kowalsky MJ. *Displacement-Based Seismic Design of Structures*. IUSS Press, Pavia, Italy, 2007.
33. Zahn FA, Park R, Priestley MJN. Flexural Strength and Ductility of Circular Hollow Reinforcement Concrete Columns without Confinement on Inside Face. *ACI Structural Journal* 1990; **87**(2):156–166.
34. Lee J-H, Choi J-H, Hwang D-K, Kwahk I-J. Seismic performance of circular hollow RC bridge columns. *KSCE Journal of Civil Engineering* 2015; **19**(5):1456–1467.
35. Lu Y, Gu X, Guan J. Probabilistic Drift Limits and Performance Evaluation of Reinforced Concrete Columns. *Journal of Structural Engineering* 2005; **131**(6):966–978.
36. Qiang H, Xiuli D, Zhou Y, Lee, GC. Experimental study of hollow rectangular bridge column performance under vertical and cyclically bilateral loads, *Earthquake Engineering and Engineering Vibration* 2013; **12**(3):433–445.
37. Delgado R, Delgado P, Vila Pouca N, Arêde A, Rocha P, Costa A. Shear effects on hollow section piers under seismic actions: Experimental and numerical analysis. *Bulletin of Earthquake Engineering* 2009; **7**(2):377–389.
38. Hannewald P, Beyer K. Plastic hinge models for the displacement-based assessment of wall-type bridge piers with poor detailing. *Proc. of Vienna Congress on Recent Advances in Earthquake Engineering and Structural Dynamics*. Vienna, Austria, 2013, paper no. 218.
39. Naeim F, Kelly JM. *Design of Seismic Isolated Structures: From Theory to Practice*. John Wiley & Sons Inc, New York, 1999.
40. Dymiotis C, Kappos AJ, Chryssanthopoulos M., Seismic Reliability of Masonry-Infilled RC Frames. *Journal of Structural Engineering (ASCE)* 2001; **127**(3):296–305.
41. Celik OC, Ellingwood BR. Seismic fragilities for non-ductile reinforced concrete frames – Role of aleatoric and epistemic uncertainties. *Structural Safety* 2010; **32**(1):1-12.
42. Vamvatsikos, D. Estimating Seismic Performance Uncertainty using IDA with Progressive Accelerogram-wise Latin Hypercube Sampling. *Proc. of 11<sup>th</sup> International Conference on Applications of Statistics and Probability in Civil Engineering*. Zurich, 2011.
43. Katsanos EI, Sextos AG. ISSARS : An intergrated software environment for structure specific earthquake ground motion selection. *Advances in Engineering Software* 2013; **58**:70–85.